JOURNAL OF GEOPHYSICAL RESEARCH, VOL. 90, NO. B10, PAGES 8563–8569, SEPTEMBER 10, 1985

Folding of Oceanic Lithosphere

DAVID C. MCADOO AND DAVID T. SANDWELL

National Geodetic Survey, Charting and Geodetic Services, National Ocean Service/NOAA
Rockville, Maryland

Folding of the lithosphere just south of the Bay of Bengal appears as (1) undulations in acoustic basement topography and (2) as linear geoid undulations in the Seasat altimeter data. From the Seasat data we find that the east-west trending folds have wavelengths ranging from 130 to 250 km and clustering about 190 km. The horizontal gravity disturbances due to the folds range in amplitude from 15 to 50 mGal. Elastic models of oceanic lithosphere have, in the past, been used to demonstrate the implausibility of lithosphere buckling, or folding, in response to compression. These elastic models typically predict that compressive stresses of about 5 GPa are required to buckle oceanic lithosphere with an age comparable to that of the northeastern Indian Ocean (40–70 Ma). These stresses exceed the strength of lithospheric rock. We use an elastic-plastic model to show that oceanic lithosphere of this age should have a net compressive strength equal to about 12% of the elastic buckling stress. We further demonstrate that loads approaching the net compressive strength cause the lithosphere to fold with a wavelength about 200 km, i.e., the wavelength observed from Seasat. Our results reinforce earlier speculation that this folding may be related to the Himalayan orogeny.

INTRODUCTION

The lithospheric plates comprising the outermost layers of the solid earth tend to remain rigid over geological time. Such rigidity is axiomatic in the hypothesis of plate tectonics. There are, however, places where significant intraplate deformations have occurred. The northeast Indian Ocean, just south of the Bay of Bengal and west of the northern Ninetyeast Ridge, is such a place. Lithospheric folding of wavelengths of 100–300 km and amplitudes approaching 3 km has apparently taken place there [*Weissel et al.*, 1980; *Geller et al.*, 1983]. This folding is manifested as undulations in the acoustic basement topography and linear anomalies in the gravity field. *Weissel et al.* [1980] speculated that this deformation of the Indo-Australian plate's interior is linked to the Himalayan orogeny. Specifically, folds whose axes trend roughly east-west arose in response to north-south horizontal compression associated with the continental collision of India and Asia. Focal mechanisms in this area are generally consistent with north-south compression [cf. *Weissel et al.*, 1980; *Geller et al.*, 1983; *Bergman and Solomon*, 1982, 1985; *Wiens*, 1985].

In contrast to most intraplate areas, this region is quite seismically active [*Sykes*, 1970]. In fact, *Stein and Okal* [1978] found that the region "is considerably more active (seismically) than the interior of any other oceanic plate." Intraplate deformation is sufficiently intense in this area to justify treating the Indo-Australian plate as two separate plates [see *Minster and Jordan*, 1978; *Stein and Gordon*, 1984]. Inasmuch as this is a region of singularly intense intraplate deformation, compressive forces are, very likely, exceptionally high.

The Seasat altimeter provides further evidence of folding of the Indo-Australian plate. Altimeter profiles of the marine geoid display prominent east-west trending undulations with amplitudes of ~ 2 m. In this study, the characteristic wavelength of these undulations is derived from 54 Seasat altimeter profiles by measuring distances between peaks and troughs. Moreover, we show that the orientations and the wavelengths of the geoid undulations agree with the seismically observed basement topography.

Paper number 4B5283.

As *Weissel et al.* [1980] indicated, it is difficult to reconcile compressive folding of the Indo-Australian plate with generally accepted elastic buckling models of the oceanic lithosphere which show that buckling cannot occur under geologically reasonable forces. The implausibility of elastic buckling in the lithosphere (crust) was first pointed out by *Smoluchowski* [1909]. See also *Heiskanen and Vening Meinesz* [1958], *Turcotte and Schubert* [1982], and *Lambeck* [1983]. *Caldwell and Turcotte* [1979], *Bodine et al.* [1981], *McAdoo et al.* [1985], and *McNutt and Menard* [1982] have postulated relations describing how the mechanical oceanic lithosphere should thicken with age. According to these relations, lithosphere in our region of study, which has an effective age (age at time of loading) of 40–70 Ma, should be 40–50 km thick. In order to produce folding or buckling in elastic lithosphere of such thickness, these compressive forces must be unduly large (i.e., equivalent to 4.9-GPa stresses). Such stresses exceed the predicted failure strength of lithospheric rock.

Recently, results from rock mechanics experiments were used to construct a yield envelope, i.e., to estimate the yield strength of the lithosphere as a function of depth [see *Goetze and Evans*, 1979; *Kirby*, 1977, 1983]. These strength estimates are based on brittle behavior of near-surface rocks and ductile behavior (thermally activated creep) at depth. When integrated over depth, the yield strength envelope produces an estimate of the net horizontal compressive strength of the lithosphere. This compressive strength is much less than the elastic buckling load. For this case, i.e., oceanic lithosphere with an effective age of 50–60 Ma, net compressive strength is about 12% of the elastic buckling load. Thus the lithosphere will fail before the compressive stress reaches the elastic buckling limit. There are at least two ways the lithosphere could fail, reverse faulting or folding.

Using an elastic-plastic yield envelope model, we demonstrate that lithospheric buckling occurs before the horizontal compressive stress reaches the strength of the lithosphere. Thus the buckling/folding mode of failure is preferred. The buckling instability develops at relatively low end loads because failure of the upper and lower lithosphere reduces the effective elastic thickness. This thinning also results in a reduction in the buckling wavelength. This very simplified model of the collision between the Indo-Australian plate and

TABLE 1. Parameters

Parameter	Definition	Value/Units
γ_B	brittle slope parameters	2.2×10^4 Pa m^{-1}*
		-6.6×10^4 Pa m^{-1}†
γ_D	ductile slope parameter (at 55 Ma)	4.8×10^4 Pa m^{-1}†
		-4.8×10^4 Pa m^{-1}*
$\dot{\varepsilon}_{01}$	Dorn law strain rate	5.7×10^{11} s^{-1}
$\dot{\varepsilon}_{02}$	power law strain rate	7.0×10^{-14} s^{-1} Pa^{-3}
$\dot{\varepsilon}_y$	characteristic strain rate	1.0×10^{-16} s^{-1}‡
E	Young's modulus	6.5×10^{10} Pa
g	acceleration of gravity	9.82 m s^{-2}
G	gravitational constant	6.67×10^{-11} N m^2 kg^{-2}
κ	thermal diffusivity	1.0×10^{-6} m^2 s^{-1}
ν	Poisson's ratio	.25
ρ_m	mantle density	3300 kg m^{-3}
ρ_s	sediment density	2300 kg m^{-3}
ρ_w	seawater density	1025 kg m^{-3}
Q_1	activation energy (Dorn)	5.35×10^5 J mol^{-1}
Q_2	activation energy (power)	5.23×10^5 J mol^{-1}
R	universal gas constant	1.99 cal mol^{-1} °K^{-1}
s	average basement depth	5.5 km
T_l	stress relaxation temp.	740°C
T_m	mantle temperature	1300°C
σ_p	Dorn law stress	8.5×10^9 Pa

*Tension.
†Compression.
‡Representative of range 10^{-15} to 10^{-17} s^{-1}.

the Asian plate produces results which agree well with observations; it predicts 200-km wavelength folds in the lithosphere. This model explains both the wavelength and amplitude of the geoid undulations as well as the folds evident in the basement topography. It is not designed to deal with the three-dimensional tectonic complexities that characterize this region [cf. *Stein and Okal*, 1978].

Elastic Buckling

The oceanic lithosphere has been modeled as a thin elastic plate (thickness of h_l) overlain by water (density of ρ_w) or sediments, floating on a fluid asthenosphere (density of ρ_m, gravitational acceleration g). Values of parameters are given in Table 1. When the elastic plate is subjected to a vertical line load $P_0\delta(x)$ and a horizontal, transverse end load F, it deflects vertically (see Figure 1) by an amount

$$w(x) = \frac{P_0}{4D\beta(\alpha^2 + \beta^2)} e^{-\beta|x|} \cos \alpha x \tag{1}$$

where x is the distance from the line load [*Hetenyi*, 1949]. The flexural rigidity D is related to the elastic thickness by

$$D = \frac{Eh_l^3}{12(1 - \nu^2)} \tag{2}$$

where E is Young's modulus and ν is Poisson's ratio. The wave numbers α and β represent length scale and spatial attenuation, respectively, where

$$\alpha = \left\{\left[\frac{g(\rho_m - \rho_w)}{4D}\right]^{1/2} + \frac{F}{4D}\right\}^{1/2} \tag{3a}$$

and

$$\beta = \left\{\left[\frac{g(\rho_m - \rho_w)}{4D}\right]^{1/2} - \frac{F}{4D}\right\}^{1/2} \tag{3b}$$

As the end load F approaches the elastic buckling limit given by

$$F_c = \left[\frac{Eh_l^3 g(\rho_m - \rho_w)}{3(1 - \nu^2)}\right]^{1/2} \tag{4}$$

the factor $\beta \to 0$. In this same limit, $F \to F_c$, deflections given by (1) become unbounded. The elastic buckling wavelength λ_c is

$$\lambda_c = 2\pi\left[\frac{Eh_l^3}{12(1 - \nu^2)g(\rho_m - \rho_w)}\right]^{1/4} \tag{5}$$

Using the elastic thickness of 46 km corresponding to a 55 Ma lithosphere (see next section, equation (9)) we find that the lithosphere buckles at a wavelength of 450 km under an average compressive stress of 4.9 GPa. This wavelength is more than twice the observed wavelength of the basement topography in the northeast Indian Ocean. Moreover, this stress exceeds the largest flexural stresses produced at outer rises of subduction zones by almost an order of magnitude [*Hanks*, 1971; *Caldwell et al.*, 1976].

The uniform elastic plate model used in this calculation is useful for describing lithosphere flexure. However, when loads are large ($\sigma > 100$ MPa), one must account for lithospheric thinning via brittle fracture and creep.

Rheology of the Lithosphere

A more appropriate model of the oceanic lithosphere is an elastic-plastic one in which yield stress is a function of depth. Using results from experimental rock mechanics as constraints, *Goetze and Evans* [1979] constructed a yield-stress envelope to represent this variation with depth. See also *Kirby* [1977]. They divided the lithosphere into three constitutive layers or regimes: a shallow cataclastic (brittle) regime, mostly crust, in which failure stress increases with pressure; a deep ductile regime, mostly upper mantle, in which yield stress decreases abruptly with increasing temperature and depth; an elastic regime which is sandwiched between the cataclastic and ductile layers. Distribution of yield strength with depth within the ductile flow regime governs the thickness, h_l, of the lithosphere. According to *Goetze and Evans* [1979] the mechanism for ductile flow and failure is one of thermally activated creep. As a result, lithospheric thickness h_l depends strongly on temperature structure, and hence age, of the lithosphere. For example, young lithosphere at any depth is relatively warm; as a result, it is relatively weak or thin.

Goetze and Evans [1979] assumed that experimentally determined steady state flow laws for olivine are appropriate for describing deformation of the upper mantle beneath the oceans. They specified two laws to represent this deformation. The first, the Dorn law,

$$\dot{\varepsilon} = \dot{\varepsilon}_{01} \exp\left[-Q_1\left(1 - \frac{\Delta\sigma}{\sigma_p}\right)^2 \Big/ RT\right] \tag{6}$$

applies when bending stress $\Delta\sigma > 2 \times 10^8$ Pa; the second, the

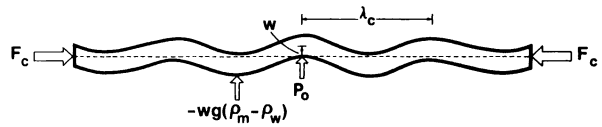

Fig. 1. Deflections $w(x)$ of an elastic lithosphere subjected to an end load F and a vertical perturbing load P_0.

power law,

$$\dot{\varepsilon} = \dot{\varepsilon}_{02}\Delta\sigma^n \exp(-Q_2/RT) \qquad n = 3 \tag{7}$$

applies when $\Delta\sigma < 2 \times 10^8$ Pa. In (6) and (7), $\dot{\varepsilon}$ is strain rate and R is the gas constant. The activation energies Q_1 and Q_2 are assigned values given by Goetze and Evans (see Table 1), as are strain rate amplitude parameters $\dot{\varepsilon}_{01}$ and $\dot{\varepsilon}_{02}$. Temperature T (in degrees Kelvin) is obtained from a thermal model of the lithosphere. *Bodine et al.* [1981] used the plate model of Parsons and Sclater [1977] to specify temperature as a function of depth in the flow laws (6) and (7). For ages of 80 Ma or less the plate thermal model is very closely approximated by the simpler half-space model [*Turcotte and Oxburgh*, 1967; *Parker and Oldenburg*, 1973]. For the study we shall use the half-space model in which temperature (in degrees Celsius) is given by

$$T = T_m \operatorname{erf}\left[\frac{z}{2(\kappa t)^{1/2}}\right] \qquad t < 80 \text{ Ma} \tag{8}$$

In (8), z is depth, t is age, κ is thermal diffusivity, and T_m is zero-age temperature (see Table 1).

The base of the lithosphere is defined by a threshold temperature above which the mechanisms of creep become efficient enough to relax appreciable (order 100 MPa) stresses. The strain rate $\dot{\varepsilon}_y$ defines the onset of yielding in the lithosphere [cf. *Goetze and Evans*, 1979]. We adopt a value of $\dot{\varepsilon}_y = 10^{-16}$ s^{-1} (see Table 1). Strain rates ranging from 10^{-17} to 10^{-15} s^{-1} produce similar results. For a fixed strain rate the shape of the yield envelope ($\Delta\sigma_y$ in Figure 1) is derived from (6), (7), and (8). To simplify subsequent bending computations, we have linearized the ductile portion of the yield envelope by fitting a straight line to the envelope through two points, $\Delta\sigma_y = 10^8$ Pa (1 kbar) and $\Delta\sigma_y = 5 \times 10^8$ Pa. The linearized yield envelope for the ductile regime is described by two parameters: (1) depth $z = h_l$, at which yield stress $\Delta\sigma_y = 10^8$ Pa and (2) slope $d\Delta\sigma_y/dz = \gamma_D$.

Using the above parameters the base of the lithosphere follows an isotherm $T_l = 740$°C. Inverting (8) the thickness is

$$h_l = C(\text{age})^{1/2} \tag{9}$$

where $C = 6.2$ km m.y.$^{-1/2}$. A similar procedure issued to solve for the slope parameter γ_D. According to our model, lithosphere of age 55 Ma has a thickness of $h = 46$ km and a slope $\gamma_D = 0.48 \times 10^5$ Pa/m. These values of h_l and γ_D are used to construct the yield envelope depicted in Figure 2.

Unlike the ductile portion of the yield envelope the cataclastic or brittle portion is invariant with respect to temperature or age of the lithosphere. This is due to the fact that the fracture strength predicted by the Coulomb law responds to increasing pressure but not to temperature. According to *Goetze and Evans* [1979] and *Bodine et al.* [1981] the fracture strength $\Delta\sigma_y$ increases linearly with overburden pressure and depth. For the brittle regime, $\Delta\sigma_y = \gamma_B z$, where $\gamma_B = 0.22 \times 10^5$ Pa/m for tensional failure and $\gamma_B = -0.66 \times 10^5$ Pa/m for compressional failure. Note that the brittle portion of the lithosphere is weaker in tension than in compression.

According to the yield envelope depicted in Figure 2 the lithosphere has a limit or saturation load F_s, which is significantly less than the elastic buckling load. Before we compute this limit load, let us first write the expression for the horizontal axial load

$$F = -\int_0^{h_l} \Delta\sigma \, dz$$

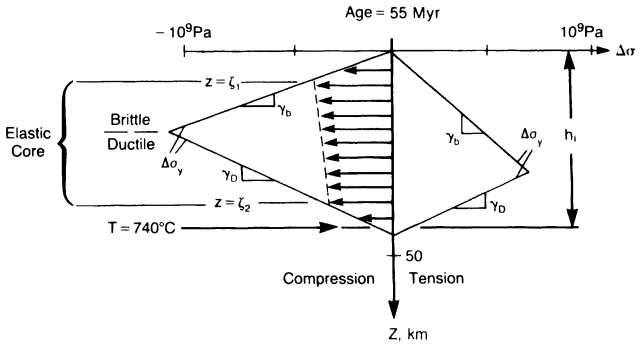

Fig. 2. Yield strength $\Delta\sigma_y$ versus depth z for elastic-plastic lithosphere of age 55 Ma Idealized from *Goetze and Evans* [1979]. Typical bending stress profile is shown (arrows) for state of net axial compression.

associated with an arbitrary stress distribution, $\Delta\sigma(z)$. For the elastic-plastic lithosphere this expression is

$$F = [\gamma_D h_l^2 - \gamma_D h_l(\zeta_1 + \zeta_2) - (\gamma_B - \gamma_D)\zeta_1\zeta_2]/2 \tag{10}$$

where for the brittle regime, $0 < z < \zeta_1$, $\Delta\sigma = \gamma_B z$, for the ductile regime, $h_l > z > \zeta_2$, $\Delta\sigma = \gamma_D(z - h_l)$, and for the elastic regime, $\zeta_1 < z < \zeta_2$, stress varies linearly between a value of $\gamma_B\zeta_1$ at $z = \zeta_1$, and $\Delta\sigma = \gamma_D(\zeta_2 - h_l)$ at $z = \zeta_2$. F is defined to be positive in compression. The limit load F_s is achieved when the elastic core vanishes, i.e.,

$$\zeta_1 = \zeta_2 = -\frac{h_l\gamma_D}{(\gamma_B - \gamma_D)}$$

From (10) we find that

$$F_s = \frac{h_l^2\gamma_B\gamma_D}{2(\gamma_B - \gamma_D)} \tag{11}$$

Elastic-Plastic Buckling

For this more realistic rheological model of the lithosphere the relationship between bending moment and curvature is nonlinear. Thus the differential equation describing lithospheric flexure due to a line load and end load is also nonlinear [see *McAdoo et al.*, 1985]. This nonlinear equation does not describe stress reversal or unloading. Our model neglects the effect of unloading on the buckling process. It also neglects the effect, on buckling, of geometric imperfections in the lithosphere. *Neale* [1975] and *Drucker and Onat* [1954] have shown that these effects may, in certain cases, significantly affect the plastic buckling process. We can linearize the moment curvature equation by expanding curvature, d^2w/dx^2, as a function of moment M in a Taylor series about zero moment. This expansion to first order yields

$$d^2w/dx^2 \doteq -M/D_E \tag{12a}$$

where

$$D_E = \frac{E(\zeta_2 - \zeta_1)^3}{12(1 - \nu^2)} \tag{12b}$$

This linearized curvature equation (12*a*) is identical to the exact curvature equation for the elastic core of thickness, $\zeta_2 - \zeta_1$. Therefore the onset of folding of the elastic-plastic lithosphere (thickness h_l) is described quite well by buckling equations for the elastic core (thickness $\zeta_2 - \zeta_1$). We have verified this by numerically solving for deflections using the exact nonlinear moment-curvature equation. The linearization in (12*a*)

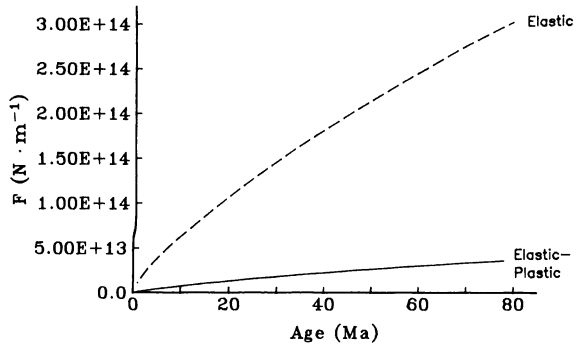

Fig. 3. Buckling load versus age for elastic-plastic lithosphere (solid curve) and for fully elastic lithosphere (dashed curve).

implies that the elastic core alone controls the deflection of the lithosphere. Actually, the entire thickness of the lithosphere controls the deflection; the elastic core idealization gives the correct effective rigidity D_E [*Drucker*, 1967, p. 416]. The apparent thinning of the elastic core results from a net horizontal intraplate loading (compressive or tensile) [*Bodine et al.*, 1981; *McAdoo and Martin*, 1984]. For the limiting case of zero curvature, it can be shown using (10) and (11) that elastic core thickness, $\zeta_2 - \zeta_1$, is given by

$$\zeta_2 - \zeta_1 = h_l(1 - F/F_s)^{1/2} \tag{13}$$

When the end load reaches the saturation load F_s, the elastic core vanishes and the lithosphere collapses. Just prior to complete failure, however, the lithosphere buckles. Adopting the linearization in (12*a*), the buckling load F_c' is found by substituting the elastic core thickness $\zeta_2 - \zeta_1$ from (13) for h_l in (4), obtaining

$$F_c' = \left[\frac{Eh_l^3(\rho_m - \rho_w)g}{3(1 - \nu^2)}\right]^{1/2}\left(1 - \frac{F_c'}{F_s}\right)^{3/4} \tag{14}$$

and then solving (14) for F_c'. Using constants appropriate to the oceanic lithosphere (see Table 1) and the lithosphere thickness h_l, given in (9), we found that the buckling load is slightly less than the limit load (i.e., $F_c'/F_s = 0.94$). Equations (9) and (11) yield F_s as a function of age. We find that F_s and hence the buckling load increase linearly with age if we ignore the weak dependence of γ_D on age. A plot of buckling load versus lithospheric age is shown in Figure 3 (solid curve). Also shown (dashed curve) is the critical buckling load for the purely elastic model (i.e., equation (4)). For all ages, the buckling load (or buckling stress) for the purely elastic model is 8–9 times greater than the buckling load (or buckling stress) for the elastic-plastic model. It is interesting to note that the gravitational sliding force, which is also proportional to the age of the lithosphere [*Lister*, 1975], is about 10 times smaller than the force needed to buckle the lithosphere. Thus the lithosphere is too strong to buckle under normal spreading conditions. However, the critical buckling force for the elastic-plastic model is, apparently, small enough to have been produced by the collision between India and Asia.

The buckling wavelength and its age dependence for the elastic-plastic model are obtained by substituting the elastic core thickness $\zeta_2 - \zeta_1$ from (13) for h_l in (5). The result is

$$\lambda_c' = 2\pi\left[\frac{Eh_l^3}{12(1 - \nu^2)g(\rho_m - \rho_w)}\right]^{1/4}\left(1 - \frac{F_c'}{F_s}\right)^{3/8} \tag{15}$$

At a given age, λ_c', shown in Figure 4 (solid curve), is about one third the buckling wavelength for the purely elastic model (dashed curve). This wavelength reduction reflects thinning of the elastic core by axial compression. Before comparing this theoretical buckling wavelength with the wavelengths of the geoid undulations, the model must be modified slightly to incorporate the effect of the sediments.

The buckling load for the elastic-plastic model (equation (14)) is nearly independent of the constants g, $\rho_m - \rho_w$, etc., since it depends primarily upon the saturation load F_s. However, the buckling wavelength (equation (15)) does depend upon these factors. In particular, a decrease in the gravitational restoring force $wg(\rho_m - \rho_w)$ increases the buckling wavelength. So far it has been assumed that the thick layer of sediments in the northeast Indian Ocean had no effect upon folding. *Weissel et al.* [1980] indicate that sediment loading occurred prior to, after, and, in all likelihood, simultaneously with the folding. If sediments were deposited as the folds developed, then the restoring force should be $wg(\rho_m - \rho_s)$. The dotted curve in Figure 4 shows the buckling wavelength when ρ_w is replaced by ρ_s in (14) and (15). For the age of the lithosphere corresponding to the Himalayan orogeny (55 Ma) the buckling wavelength for the elastic-plastic model lies between 160 and 240 km. This range is significantly less than the range for the purely elastic model (370–550 km).

Recall that our expressions (14) and (15) for critical buckling load F_c' and critical buckling wavelength λ_c', respectively, are obtained by using a linearized approximation (equation (12*a*)) of the deflection equation. As it happens, this linearization produces good estimates of the load F_c' and the wavelength λ_c'. This can be verified by solving numerically the nonlinear deflection equation. It can be more crudely verified by noting that estimates of critical buckling load F_c' are roughly equal to the limit load F_s and that the estimated buckling wavelength λ_c' is nearly equal to the buckling wavelength of a fully elastic lithosphere whose critical buckling load is equal to F_s. However, we can demonstrate, a posteriori, that this linearization produces estimates of core thickness $\zeta_2 - \zeta_1$ at buckling which are somewhat large (i.e., about one fifth the full thickness h_l). In fact, elastic core thickness at buckling will vary with position x and should be of order one tenth the full thickness h_l.

Seasat Data

Evidence for folding of the Indo-Australian plate has been found (see the introduction) in the three types of data, seismic reflections, surface gravity, and satellite altimetry. All three

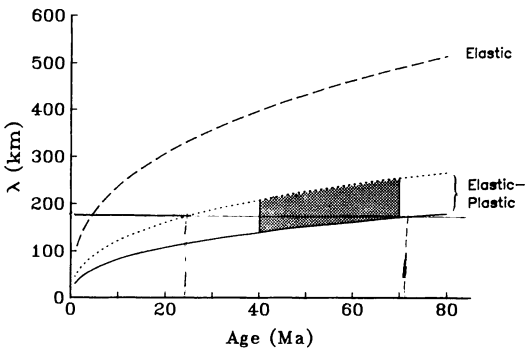

Fig. 4. Buckling wavelength versus age for elastic-plastic lithosphere without sediment loading (solid curve), with sediment loading (dotted curve); dashed curve depicts buckling wavelength for fully elastic lithosphere.

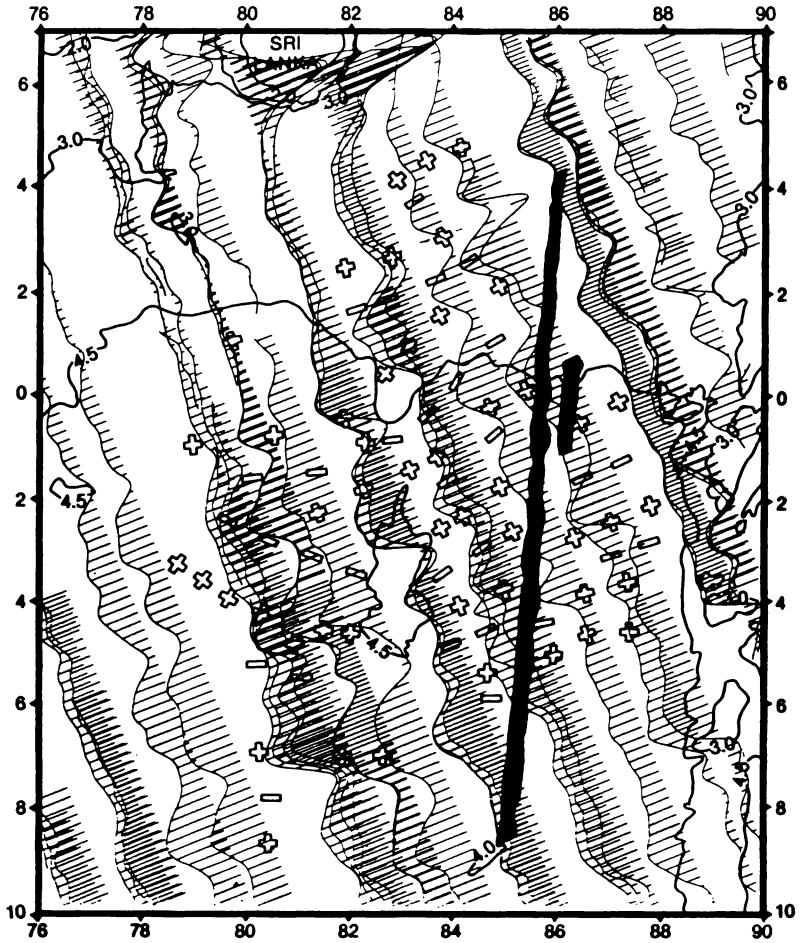

Fig. 5. Along-track deflections of the vertical for ascending Seasat altimeter passes. Scale: 40 μrad/degree of longitude. Also shown is topography of acoustic basement from *Geller et al.* [1983]. Plus signs are relative highs; minus signs are lows.

types of data suggest 1–3 km folds with wavelength ranging from 100 to 300 km [*Weissel et al.*, 1980]. Recently, *Weissel and Haxby* [1982] were able to predict the seafloor and basement topography in the Indian Ocean from Seasat altimeter data by assuming that the topography was uncompensated. By making this assumption, the Fourier transform of the deflection of the vertical is

$$\eta(k) = \frac{2\pi G(\rho_m - \rho_s) ik\, e^{-|k|s}}{g|k|} W(k) \qquad (16)$$

where G is the gravitational constant, s is the depth to the topography, $W(k)$ is the Fourier transform of the topography, and k is 2π/wavelength. At buckling, the topography is sinusoidal and of wavelength λ_c' given in (15). From (16) then the deflections of the vertical (or horizontal gravity disturbances) are also sinusoidal, also of wavelength λ_c', but are phase shifted by 90° with respect to topography. The amplitude of the sinusoid representing deflections of the vertical is simply Z times the amplitude of topography where

$$Z = \frac{2\pi G(\rho_m - \rho_s)}{g} e^{-2\pi s/\lambda_c'} \qquad (17)$$

Using the constants in Table 1 and a buckling wavelength of 200 km, this ratio Z is 36 μrad/km. Where the sediments are thin, ρ_s should be replaced by ρ_w. In this case the ratio is higher, 83 μrad/km.

To obtain a more accurate value for the characteristic folding wavelength, we examined all of the Seasat passes in the area. Plots of along-track deflection of the vertical for ascending Seasat profiles are shown in Figure 5. These profiles are superimposed upon the basement topography map of *Geller et al.* [1983]. The Seasat data were processed in the following manner: (1) each profile was differentiated, (2) the PGSS4 gravity model [*Marsh and Martin*, 1982], to degree and order 36, was subtracted from each pass, and (3) each profile was low-pass filtered with a Gaussian-shaped filter, half width of 35 km. This procedure effectively removes undulations outside the wavelength band from 35 to 1000 km; it also "whitens" the spectrum.

In Figure 5 the data are displayed along the subsatellite track. Deviations from the track represent deflections of the vertical (scale = 40 μrad/degree of longitude). For every other data point a straight line connects the subsatellite track with the deflection curve. Deflection variations associated with folding range, in amplitude, from 15 to 50 μrad; equivalently, horizontal gravity disturbances vary in amplitude from 15 to 50 mGal.

Figure 6 is an illuminated relief map of the marine geoid (mean sea surface) over the Indian Ocean. This map was derived from Seasat and Geos 3 data by *Marsh et al.* [1984]. It shows east-west trending undulations in the geoid over our region of study just south of the Bay of Bengal. These undu-

Fig. 6. An illuminated relief map of the marine geoid (mean sea surface) constructed from Seasat and Geos 3 data by *Marsh et al.* [1984].

lations are the same features which dominate the deflection-of-the-vertical profiles in Figure 5; they are associated with the lithospheric folding.

To determine the characteristic wavelength of the undulations, we measured distances between adjacent relative maxima along the ascending and descending deflection profiles. Similarly, we measured distances between adjacent relative minima. The distances were then projected perpendicular to the trends apparent in the basement topography [*Geller et al.*, 1983]. Data near Sri Lanka, the Ninetyeast Ridge, and the fracture zone at 85°E were not used. The results are shown as a histogram of wavelengths in Figure 7. Most of the undulations have wavelengths between 130 and 250 km with the highest number of occurrences at a wavelength of 190 km. The arrows in Figure 7 mark the range of buckling wavelengths predicted by the elastic-plastic model.

Discussion

We have attempted to model, very simply, the intense intraplate deformation or folding of the Indo-Australian plate. Folding of mature oceanic lithosphere is quite unusual. Folding is more typical of continental lithosphere. Our simple model of this folding predicts that thickness averaged compressive stresses reach 600 MPa (6 kbar). Such stresses are large, but large stresses are to be expected for this unique region of very intense deformation (see *Hanks and Raleigh* [1980] for a discussion of intraplate stress levels). Furthermore, these stresses are acceptable from the viewpoint of

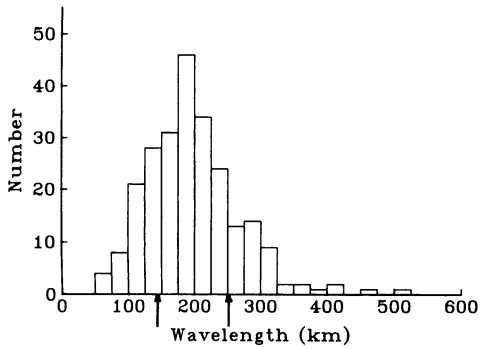

Fig. 7. Histograms of undulation wavelengths from Seasat altimeter data over northeastern Indian Ocean. Arrows depict buckling wavelength range predicted by model.

experimental rock mechanics inasmuch as our model of lithospheric strength is based on the results of these experimental studies.

In addition to predicting a very reasonable spatial wavelength of folding, the model predicts a reasonable stress distribution: specifically, it predicts that for moderate amplitude folds like those beneath the Indian Ocean, deviatoric stresses be compressional throughout the lithosphere. This absence of deviatoric tensional stress is consistent with the complete absence of normal faulting earthquakes [see *Bergman and Solomon*, 1985].

Summary

Observations of basement topography and geoid height indicate that the oceanic lithosphere in the northern Indian Ocean folded under axial compression caused by the collision of India and Asia. These ideas are inconsistent with purely elastic buckling theory for two reasons: (1) the buckling force is unrealistically high and (2) the buckling wavelength is twice as large as those observed. An elastic-plastic model of the oceanic lithosphere, based upon experimental rock mechanics, predicts folding at wavelengths of 200 km in agreement with those observed in Seasat altimeter data. The model requires an average compressive stress of only 600 MPa to buckle moderately old lithosphere. The success of the model indicates that compressional forces are responsible for some of the topography formed away from plate boundaries.

Acknowledgments. We thank Carol Stein of Northwestern University for discussions and for providing a seafloor map. Helpful discussions with Chreston Martin of EG&G are gratefully acknowledged. Eric Bergman volunteered some constructive criticism. Seth Stein and Sean Solomon provided helpful reviews. We are indebted to Jim Marsh for providing the altimetric sea surface image used in Figure 6.

References

Bergman, E. A., and S. C. Solomon, Recent studies in Indian Ocean intraplate seismicity (abstract), *Eos Trans. AGU*, *63*, 1092, 1982.

Bergman, E. A., and S. C. Solomon, Earthquake source mechanisms from body-waveform inversion and intraplate tectonics in the northern Indian Ocean, *Earth Planet. Inter.*, in press, 1985.

Bodine, J. H., M. S. Steckler, and A. B. Watts, Observations of flexure and the rheology of the oceanic lithosphere, *J. Geophys. Res.*, *86*, 3695–3707, 1981.

Caldwell, J. G., and D. L. Turcotte, Dependence of the thickness of the elastic oceanic lithospheric on age, *J. Geophys. Res.*, *84*, 7572–7576, 1979.

Caldwell, J. G., W. F. Haxby, D. E. Karig, and D. L. Turcotte, On the applicability of a universal elastic trench profile, *Earth Planet. Sci. Lett.*, *31*, 239–246, 1976.

Drucker, D. C., *Introduction to Mechanics of Deformable Solids*, McGraw-Hill, New York, 1967.

Drucker, D. C., and E. T. Onat, On the concept of stability of inelastic systems, *J. Aeronaut. Sci.*, *21*, 543–548, 1954.

Geller, C. A., J. K. Weissel, and R. N. Anderson, Heat transfer and intraplate deformation in the central Indian Ocean, *J. Geophys. Res.*, *88*, 1018–1032, 1983.

Goetze, C., and B. Evans, Stress and temperature in the bending lithosphere as constrained by experimental rock mechanics, *Geophys. J. R. Astron. Soc.*, *59*, 463–478, 1979.

Hanks, T. C., The Kuril Trench–Hokkaido Rise system: Large shallow earthquakes and simple models of deformation, *Geophys. J. R. Astron. Soc.*, *23*, 173–189, 1971.

Hanks, T. C., and C. B. Raleigh, The conference on magnitude of deviatoric stresses in the earth's crust and uppermost mantle, *J. Geophys. Res.*, *85*, 6083–6085, 1980.

Heiskanen, W. A., and F. A. Vening Meinesz, *The Earth and Its Gravity Field*, pp. 318–319, McGraw-Hill, New York, 1958.

Hetenyi, M., *Beams on Elastic Foundation*, University of Michigan Press, Ann Arbor, 1949.

Kirby, S. H., State of stress in the lithosphere: Inferences from the flow laws of olivine, *Pure Appl. Geophys.*, *115*, 245–258, 1977.

Kirby, S. H., Rheology of the lithosphere, *Rev. Geophys.*, *21*, 1458–1487, 1983.

Lambeck, K., The role of compressive forces in intracratonic basin formation and mid-plate orogenies, *Geophys. Res. Lett.*, *10*, 845–848, 1983.

Lister, C. R. B., Gravitational drive on oceanic plates caused by thermal contraction, *Nature*, *257*, 663–665, 1975.

Marsh, J. G., and T. V. Martin, The Seasat altimeter mean sea surface model, *J. Geophys. Res.*, *87*, 3269–3280, 1982.

Marsh, J. G., C. J. Koblinsky, A. Brenner, B. Beckley, and T. Martin, Global mean sea surface computations based upon a combination of Seasat and Geos-3 satellite altimeter data (abstract), *Eos Trans. AGU*, *65*(45), 857, 1984.

McAdoo, D. C., and C. F. Martin, Seasat observations of lithospheric flexure seaward of trenches, *J. Geophys. Res.*, *89*, 3201–3210, 1984.

McAdoo, D. C., C. F. Martin, and S. Poulose, Seasat observations of flexure: Evidence for a strong lithosphere, *Tectonophysics*, in press, 1985.

McNutt, M. K., and H. W. Menard, Constraints on yield strength in the oceanic lithosphere derived from observations of flexure, *Geophys. J. R. Astron. Soc.*, *71*, 363–394, 1982.

Minster, J. B., and T. H. Jordan, Present-day plate motions, *J. Geophys. Res.*, *83*, 5331–5354, 1978.

Neale, K. W., Effect of imperfections on the plastic buckling of rectangular plates, *J. Appl. Mech.*, 115–120, 1975.

Parker, R. L., and D. W. Oldenburg, Thermal model of oceanic ridges, *Nature Phys. Sci.*, *242*, 137–139, 1973.

Parsons, B., and J. G. Sclater, An analysis of the variation of ocean floor bathymetry with age, *J. Geophys. Res.*, *82*, 803–827, 1977.

Smoluchowski, M., Uber ein gewisses Stabilitatsproblem der Elastizitatslehre und dessen Beziehung zur Entstehung von Faltengebirgen, *Bull. Int. Acad. Sci. Cracovie*, *00*, 3–20, 1909.

Stein, S., and R. G. Gordon, Statistical tests of additional plate boundaries from plate motion inversions, *Earth Planet. Sci. Lett.*, *69*, 401–412, 1984.

Stein, S., and E. A. Okal, Seismicity and tectonics of the Ninetyeast Ridge area: Evidence for internal deformation of the Indian plate, *J. Geophys. Res.*, *83*, 2233–2246, 1978.

Sykes, L. R., Seismicity of the Indian Ocean and a possible nascent island arc between Ceylon and Australia, *J. Geophys. Res.*, *75*, 5041–5055, 1970.

Turcotte, D. L., and E. R. Oxburgh, Finite amplitude convection cells and continental drift, *J. Fluid Mech.*, *28*, 29–42, 1967.

Turcotte, D. L., and G. Schubert, *Geodynamics*, pp. 124–125, John Wiley, New York, 1982.

Weissel, J. K., and W. F. Haxby, Predicting seafloor topography from Seasat altimeter data using isostatic models (abstract), *Eos Trans. AGU*, *63*(45), 907, 1982.

Weissel, J. K., R. N. Anderson, and C. A. Geller, Deformation of the Indo-Australian plate, *Nature*, *287*, 284–291, 1980.

Wiens, D., Historical Seismicity near Chagos: Deformation of the equatorial region of the Indo-Australian plate, *Earth Planet. Sci. Lett.*, in press, 1985.

D. C. McAdoo and D. T. Sandwell, Geodetic Research and Development Laboratory, National Geodetic Survey, Charting and Geodetic Services, NOAA/National Ocean Service, N/Cg113, Rockville, MD 20852.

(Received September 20, 1984;
revised March 4, 1985;
accepted April 15, 1985.)